

**TEMPERATURE-DEPENDENT PHASE TRANSITION STUDIES
AND INFLUENCE OF HYDROGEN BONDING INTERACTIONS
ON THE STRUCTURAL AND PACKING MODES OF ORGANIC
MOLECULES IN SINGLE CRYSTALLINE STATE**

Quah Ching Kheng

**UNIVERSITI SAINS MALAYSIA
2011**

**TEMPERATURE-DEPENDENT PHASE TRANSITION STUDIES
AND INFLUENCE OF HYDROGEN BONDING INTERACTIONS
ON THE STRUCTURAL AND PACKING MODES OF ORGANIC
MOLECULES IN SINGLE CRYSTALLINE STATE**

by

MR QUAH CHING KHENG

**Thesis submitted in fulfillment of the requirements
for the degree of
Doctor of Philosophy**

April 2011

ACKNOWLEDGEMENT

I would like to express my sincere thanks to my principal supervisor, Professor Fun Hoong-Kun and my co-supervisor, Associate Professor Ong Lye-Hock, my co-supervisor, without them, this research would not be successful. I express my deep sense of gratitude for their professionalism, unconditional commitment and patient throughout my study. Special thanks are due to my parents and brothers, Quah Chin Boon, Goh Suan Choo, Quah Ching Lee and Quah Chin Beng for their support and understanding. My sincere thanks are due to Dr Madhukar Hemamalini, Dr Samuel Robinson Jebas and Dr Reza Kia, postdoctoral research fellows at X-ray Crystallography Unit, School of Physics, Universiti Sains Malaysia who have given me lots of useful ideas and advices throughout my study. Appreciation is extended to the Malaysian Government and Universiti Sains Malaysia (USM) for the research fellowship and Research Officer position through the Science Fund grant No. 305 / PFIZIK / 613312. Last but not least, I would like to express my heartfelt gratitude to Mr Mohd. Mustaqim Rosli, Mr Karunakaran, Mr Mohamed Mustaqim and my fellow friends for their very kind help and warm hospitality. I am lucky to be a member of X-ray crystallography group and I shall treasure every memorable moment (Beijing Normal University visit, Thailand trip and countless gathering) we had together. Best friends forever!

TABLE OF CONTENTS

	Page
Acknowledgement	ii
Table of Contents	iii
List of Tables	xi
List of Figures	xv
List of Plates	xx
List of Abbreviations	xxi
Abstrak	xxii
Abstract	xxiv
 CHAPTER 1 INTRODUCTION	
1.1 General Introduction to Hydrogen Bonding and Other Interactions in the Crystalline State.	2
1.2 X-ray Crystallography Technique	6
1.3 Brief Description on Phase Transition	11
1.4 Samples Prepared for Phase Transition Studies	12
1.4.1 Hexamethylenetetraminium p-nitrobenzoate	13
1.4.2 2,4,4'-Trimethoxybenzophenone	13
1.4.3 4-Aminopyridinium 4-nitrobenzoic acid 4-nitrobenzoate	14
1.4.4 2-Aminopyridinium 4-hydroxybenzoate	14
1.4.5 3-Aminobenzoic acid 4-nitrobenzoic acid (1/1)	14
1.4.6 2-Amino-5-bromopyridine 4-hydroxybenzoic acid	15

1.4.7	2-Amino-4-methyl-pyridinium 3, 5-dinitrosalicylate	15
1.4.8	2-Amino-4-methylpyridinium 2-carboxybenzoate	16
1.4.9	Bis (4-aminopyridinium) Sulfate Monohydrate	16
1.4.10	2-Amino-5-bromopyridinium 2-Hydroxybenzoate	17
1.4.11	2-Amino-5-methylpyridinium 2-Hydroxybenzoate	17
1.4.12	Bis(2-amino-5-bromopyridinium) Fumarate Dihydrate	18
1.4.13	2-Amino-5-bromopyridinium 2-Carboxybenzoate	18
1.4.14	8-Hydroxyquinolinium 2-Carboxyacetate	19
1.4.15	Quinoline-2-carbonitrile-fumaric Acid (1/0.5)	19
1.5	Research Objectives	19

CHAPTER 2 FUNDAMENTAL OF X-RAY STRUCTURE ANALYSIS

2.1	X-ray Diffraction	21
2.2	Intensity of Reflections	23
2.3	Atomic Scattering Factors	23
2.4	Argand Diagram	25
2.5	Combination of N Waves	27
2.6	Phase Difference	28
2.7	Structure Factor $F(hkl)$	28
2.8	Systematic Absences	30
2.9	Friedel's Law	33
2.10	Fourier Maps Calculation	35
2.11	Heavy Atom or Patterson Methods	37
2.11.1	The Patterson Map and Patterson Function	37
2.11.2	One-Dimensional Patterson Function	38

2.11.3	Three-Dimensional Patterson Function	39
2.11.4	Positions and Weights of Peaks in the Patterson Function	39
2.11.5	Sharpened Patterson Function	41
2.11.6	Partial Fourier Synthesis	42
2.11.7	Successive Fourier Refinement	43
2.11.8	Difference-Fourier Synthesis	44
2.12	Direct Methods	45
2.13	Refinement	49
2.14	Laudau Theory of Phase Transition	51
2.14.1	Classification of Phase Transitions	52
2.14.2	Ferroelastic Phase Transition	53
2.14.3	Crystal Symmetry Breaking Involves in Ferroelastic Materials	55
2.14.4	Laudau Theory in General for Ferroelastic Phase Transition	56
CHAPTER 3 EQUIPMENTS AND METHODOLOGY		
3.1	Equipment and Software.	58
3.1.1	Bruker SMART APEX II and APEX II DUO Diffractometers.	58
3.1.2	Oxford Cryosystem Cobra Low-temperature Attachment	64
3.1.3	Software	65
3.2	Synthesization and Crystallization.	66
3.2.1	Preparation of Hexamethylenetetraminium P-nitrobenzoate.	67
3.2.2	Preparation of 2,4,4'-Trimethoxybenzophenone	67
3.2.3	Preparation of 4-Aminopyridinium 4-Nitrobenzoic Acid 4-Nitrobenzoate	67
3.2.4	Preparation of 2-Aminopyridinium 4-Hydroxybenzoate	67

3.2.5	Preparation of 3-Aminobenzoic Acid 4-Nitrobenzoic Acid (1/1)	68
3.2.6	Preparation of 2-Amino-5-bromopyridine 4-Hydroxybenzoic Acid	68
3.2.7	Preparation of 2-Amino-4-ethyl-pyridinium 3,5-dinitrosalicylate	68
3.2.8	Preparation of 2-Amino-4-methylpyridinium Hydrogen Phthalate	68
3.2.9	Preparation of Bis (4-aminopyridinium) Sulfate Monohydrate	69
3.2.10	Preparation of 2-Amino-5-bromopyridinium 2-Hydroxybenzoate	69
3.2.11	Preparation of 2-Amino-5-methylpyridinium 2-Hydroxy benzoate	69
3.2.12	Preparation of 2-Amino-5-bromopyridinium Fumarate (1/2) Monohydrate	69
3.2.13	Preparation of 2-Amino-5-bromopyridinium Hydrogen phthalate	70
3.2.14	Preparation of 8-Hydroxyquinolinium 2-Carboxyacetate	70
3.2.15	Preparation of Quinoline-2-carbonitrile-fumaric Acid (1/0.5)	70
3.3	Data Collection and Reduction	70
3.3.1	Data Collection	71
3.3.2	Data Reduction and Correction	72
3.4	Structure Determination	73
3.4.1	Space Group Determination -XPREP	73
3.4.2	Solving by Direct Methods – XS	74
3.4.3	Interactive Molecular Graphics	74
3.4.4	Least-squares Structure Refinement	75
3.4.5	Absorption Correction	77
3.4.6	Material Preparation for Crystal Structure Report	77
3.4.7	Intra- and Intermolecular Interactions Studies	78

3.4.8	Ring Conformations	79
3.5	Phase transition phenomenon determination	81
CHAPTER 4 RESULTS AND DISCUSSION		
4.1	Temperature Dependent Order-disorder Multiple Phase Transitions Studies of the Hexamethylenetetraminium P-nitrobenzoate (I) Co-crystal	83
4.1.1	Introduction	85
4.1.2	Data Collection	87
4.1.3	Refinement	89
4.1.4	Discussion	89
4.1.4.1	Ferroelastic Transition from Monoclinic Cm to Cc (First Transition).	89
4.1.4.2	Structural Disordered to Ordered Phase Transition from Monoclinic Cc to Cc (Second Transition).	90
4.1.4.3	Crystallography Results	91
4.1.5	Hydrogen Bonding Patterns and Crystal Packing	97
4.1.6	Landau Theory of Phase Transition in Adduct I	105
4.2	Temperature-dependent Isomorphous Phase Transition Studies in Molecular Crystals of 2,4,4'-Trimethoxybenzophenone (II).	112
4.2.1	Data Collection	112
4.2.2	Refinement	112
4.2.3	Discussion	113
4.2.4	Hydrogen Bonding Patterns and Crystal Packing	116
4.2.5	Landau Theory Approach of Phase Transition in Compound II	123
4.3	4-Aminopyridinium 4-Nitrobenzoic Acid 4-Nitrobenzoate (III)	131
4.3.1	Data Collection	131
4.3.2	Refinement	131

4.3.3	Discussion	132
4.3.4	Hydrogen Bonding Patterns and Crystal Packing	133
4.4	2-Aminopyridinium 4-Hydroxybenzoate (IV)	137
4.4.1	Data Collection	137
4.4.2	Refinement	137
4.4.3	Discussion	138
4.4.4	Hydrogen Bonding Patterns and Crystal Packing	139
4.5	3-Aminobenzoic Acid 4-Nitrobenzoic Acid (1/1) (V)	142
4.5.1	Data Collection	142
4.5.2	Refinement	142
4.5.3	Discussion	143
4.5.4	Hydrogen Bonding Patterns and Crystal Packing	144
4.6	2-Amino-5-bromopyridine 4-Hydroxybenzoic Acid (VI)	147
4.6.1	Data Collection	147
4.6.2	Refinement	147
4.6.3	Discussion	148
4.6.4	Hydrogen Bonding Patterns and Crystal Packing	150
4.7	2-Amino-4-methyl-pyridinium 3, 5-Dinitrosalicylate (VII)	153
4.7.1	Data Collection	153
4.7.2	Refinement	153
4.7.3	Discussion	154
4.7.4	Hydrogen Bonding Patterns and Crystal Packing	156
4.8	2-Amino-4-methylpyridinium 2-carboxybenzoate (VIII)	159
4.8.1	Data Collection	159
4.8.2	Refinement	159

4.8.3	Discussion	160
4.8.4	Hydrogen Bonding Patterns and Crystal Packing	161
4.9	Bis(4-aminopyridinium) Sulfate Monohydrate (IX)	164
4.9.1	Data Collection	164
4.9.2	Refinement	164
4.9.3	Discussion	165
4.9.4	Hydrogen Bonding Patterns and Crystal Packing	166
4.10	2-Amino-5-bromopyridinium 2-Hydroxybenzoate (X)	170
4.10.1	Data Collection	170
4.10.2	Refinement	170
4.10.3	Discussion	171
4.10.4	Hydrogen Bonding Patterns and Crystal Packing	172
4.11	2-Amino-5-methylpyridinium 2-Hydroxybenzoate (XI)	175
4.11.1	Data Collection	175
4.11.2	Refinement	175
4.11.3	Discussion	176
4.11.4	Hydrogen Bonding Patterns and Crystal Packing	177
4.12	Bis(2-amino-5-bromopyridinium) fumarate dihydrate (XII)	180
4.12.1	Data Collection	180
4.12.2	Refinement	180
4.12.3	Discussion	181
4.12.4	Hydrogen Bonding Patterns and Crystal Packing	182
4.13	2-Amino-5-bromopyridinium 2-Carboxybenzoate (XIII)	185
4.13.1	Data Collection	185
4.13.2	Refinement	185

4.13.3	Discussion	186
4.13.4	Hydrogen Bonding Patterns and Crystal Packing	188
4.14	8-Hydroxyquinolinium 2-Carboxyacetate (XIV)	190
4.14.1	Data Collection	190
4.14.2	Refinement	190
4.14.3	Discussion	191
4.14.4	Hydrogen Bonding Patterns and Crystal Packing	192
4.15	Quinoline-2-carbonitrile–fumaric acid (1/0.5) (XV)	195
4.15.1	Data Collection	195
4.15.2	Refinement	195
4.15.3	Discussion	196
4.15.4	Hydrogen Bonding Patterns and Crystal Packing	197
 CHAPTER 5 CONCLUSION		
5.1	Conclusion	200
5.2	Recommendation for Further Work	202
 REFERENCES		
LIST OF PUBLICATION		
		211

LIST OF TABLES

	Page
Table 1.1 Example of hydrogen bond table	4
Table 1.2 Properties of strong, moderate and weak hydrogen bonding interactions	4
Table 1.3 Typical enthalpies of hydrogen bond	5
Table 2.1 Limiting conditions for unit cell type	32
Table 2.2 Limiting conditions for 2_1 screw axes	33
Table 2.3 Limiting conditions for glide planes	33
Table 4.1 Summary of crystallographic data and refinement for hexamethylenetetraminium p-nitrobenzoate co-crystal	84
Table 4.2 Selected bond lengths for hexamethylenetetraminium p-nitrobenzoate co-crystal at 290 K	92
Table 4.3 Selected bond lengths for hexamethylenetetraminium p-nitrobenzoate co-crystal at 195 K	93
Table 4.4 Selected bond lengths for hexamethylenetetraminium p-nitrobenzoate co-crystal at 100 K	94
Table 4.5 The puckering parameters of the six-membered C-N-C-N-C-N rings of the hexamethylenetetraminium cations	96
Table 4.6 Hydrogen-bond geometry (\AA , $^\circ$) for HMTA-PBNA at 290 K	98
Table 4.7 Hydrogen-bond geometry (\AA , $^\circ$) for HMTA-PBNA at 195 K	98
Table 4.8 Hydrogen-bond geometry (\AA , $^\circ$) for HMTA-PBNA at 100 K	99
Table 4.9 Summary of crystallographic data and refinement for 2,4,4'-trimethoxybenzophenone	113
Table 4.10 Selected bond lengths for 2,4,4'-trimethoxybenzophenone at 297 K	114
Table 4.11 Selected bond lengths for 2,4,4'-trimethoxybenzophenone at 100 K	115
Table 4.12 Hydrogen-bond geometry for 2,4,4'-trimethoxybenzophenone at 297 K	117

Table 4.13	Hydrogen-bond geometry for 2,4,4'-trimethoxybenzophenone at 100 K	118
Table 4.14	Inter-planar angles between aromatic and functional groups in 2,4,4'-trimethoxybenzophenone at 100 K	118
Table 4.15	Inter-planar angles between aromatic and functional groups in 2,4,4'-trimethoxybenzophenone at 297 K	118
Table 4.16	Temperature dependence of <i>a</i> , <i>b</i> , <i>c</i> -axes, angles and volume of 2,4,4'-trimethoxybenzophenone	128
Table 4.17	Summary of crystallographic data and refinement for 4-aminopyridinium 4-nitrobenzoic acid 4-nitrobenzoate	132
Table 4.18	Selected bond lengths for 4-aminopyridinium 4-nitrobenzoic acid 4-nitrobenzoate	134
Table 4.19	Hydrogen-bond geometry for 4-aminopyridinium 4-nitrobenzoic acid 4-nitrobenzoate	135
Table 4.20	Summary of crystallographic data and refinement for 2-aminopyridinium 4-hydroxybenzoate	138
Table 4.21	Selected bond lengths for 2-aminopyridinium 4-hydroxybenzoate	139
Table 4.22	Hydrogen-bond geometry for 2-aminopyridinium 4-hydroxybenzoate	140
Table 4.23	Summary of crystallographic data and refinement for 3-aminobenzoic acid 4-nitrobenzoic acid (1/1)	143
Table 4.24	Selected bond lengths for 3-aminobenzoic acid 4-nitrobenzoic acid (1/1)	144
Table 4.25	Hydrogen-bond geometry for 3-aminobenzoic acid 4-nitrobenzoic acid (1/1)	145
Table 4.26	Summary of crystallographic data and refinement for 2-amino-5-bromopyridine 4-hydroxybenzoic acid	148
Table 4.27	Selected bond lengths for 2-amino-5-bromopyridine 4-hydroxybenzoic acid	149
Table 4.28	Hydrogen-bond geometry (Å, °) for 2-amino-5-bromopyridine 4-hydroxybenzoic acid	150

Table 4.29	Summary of crystallographic data and refinement for 2-amino-4-methyl-pyridinium 3, 5-dinitrosalicylate	154
Table 4.30	Selected bond lengths for 2-amino-4-methyl-pyridinium 3, 5-dinitrosalicylate	155
Table 4.31	Hydrogen-bond geometry for 2-amino-4-methyl-pyridinium 3, 5-dinitrosalicylate	156
Table 4.32	Summary of crystallographic data and refinement for 2-amino-4-methylpyridinium 2-carboxybenzoate	160
Table 4.33	Selected bond lengths for 2-amino-4-methylpyridinium 2-carboxybenzoate	161
Table 4.34	Hydrogen-bond geometry for 2-amino-4-methylpyridinium 2-carboxybenzoate	162
Table 4.35	Summary of crystallographic data and refinement for bis(4-aminopyridinium) sulfate monohydrate	165
Table 4.36	Selected bond lengths for bis(4-aminopyridinium) sulfate monohydrate	166
Table 4.37	Hydrogen-bond geometry for bis(4-aminopyridinium) sulfate monohydrate	167
Table 4.38	Summary of crystallographic data and refinement for 2-amino-5-bromopyridinium 2-hydroxybenzoate	171
Table 4.39	Selected bond lengths for 2-amino-5-bromopyridinium 2-hydroxybenzoate	172
Table 4.40	Hydrogen-bond geometry for 2-amino-5-bromopyridinium 2-hydroxybenzoate	173
Table 4.41	Summary of crystallographic data and refinement for 2-amino-5-methylpyridinium 2-hydroxybenzoate	176
Table 4.42	Selected bond lengths for 2-amino-5-methylpyridinium 2-hydroxybenzoate	177
Table 4.43	Hydrogen-bond geometry for 2-amino-5-methylpyridinium 2-hydroxybenzoate	178
Table 4.44	Summary of crystallographic data and refinement for bis(2-amino-5-bromopyridinium) fumarate dihydrate	181
Table 4.45	Selected bond lengths for bis(2-amino-5-bromopyridinium) fumarate dihydrate	182

Table 4.46	Hydrogen-bond geometry for bis(2-amino-5-bromo pyridinium) fumarate dihydrate	183
Table 4.47	Summary of crystallographic data and refinement for 2-amino-5-bromopyridinium 2-carboxybenzoate	186
Table 4.48	Selected bond lengths for 2-amino-5-bromopyridinium 2-carboxybenzoate	187
Table 4.49	Hydrogen-bond geometry for 2-amino-5-bromopyridinium 2-carboxybenzoate	188
Table 4.50	Summary of crystallographic data and refinement for 8-hydroxyquinolinium 2-carboxyacetate	191
Table 4.51	Selected bond lengths for 8-hydroxyquinolinium 2-carboxyacetate	192
Table 4.52	Hydrogen-bond geometry for 8-hydroxyquinolinium 2-carboxyacetate	193
Table 4.53	Summary of crystallographic data and refinement for quinoline-2-carbonitrile–fumaric acid (1/0.5)	196
Table 4.54	Selected bond lengths for quinoline-2-carbonitrile–fumaric acid (1/0.5)	197
Table 4.55	Hydrogen-bond geometry for quinoline-2-carbonitrile–fumaric acid (1/0.5)	199

LIST OF FIGURES

		Page
Figure 1.1	Diagram illustrating X-ray diffraction techniques	6
Figure 1.2	Diagram illustrating Miller indices	9
Figure 1.3	Cross section of filament X-ray tube	10
Figure 2.1	Diagram illustrating X-ray diffraction	22
Figure 2.2	Atomic scattering factors (a) stationary atom, $f_{j, \theta}$ (b) atom corrected for thermal vibration, $f_{j, \theta} T_{j, \theta}$	24
Figure 2.3	Combination of two waves as vectors on an Argand diagram	26
Figure 2.4	Combination of N waves ($N = 6$) using an Argand diagram	27
Figure 2.5	Structure factor $F(hkl)$ plotted on an Argand diagram	29
Figure 2.6	Relationship between $F(hkl)$ dan $F(\bar{h}\bar{k}\bar{l})$ leading to Friedel's law	34
Figure 2.7	Effect of sharpening on the radial decrease of the local average intensity $ \overline{F_o} ^2$	41
Figure 2.8	Partial structure phasing	42
Figure 2.9	Classification of phase transitions diagram	53
Figure 3.1	SMART APEX II scheme	59
Figure 3.2	SMART goniometer components	59
Figure 3.3	APEX II software diagram	66
Figure 3.4	Conformations observed for six-member rings	80
Figure 3.5	Conformations observed for five-member rings	81
Figure 3.6	Conformations observed for eight-member rings	81
Figure 4.1	The schematic diagram of order-disorder multiple phase transitions observed in p-nitrobenzoate anions	83
Figure 4.2	Schematic diagram of hexamethylenetetraminium p-nitrobenzoate co-crystal	85

Figure 4.3A	Temperature dependence of <i>a</i> -, <i>b</i> - and <i>c</i> -axes lengths of the adduct I.	88
Figure 4.3B	Temperature dependence β angle and (c) volume of the adduct I.	88
Figure 4.3C	Temperature dependence of volume of the adduct I	88
Figure 4.4A	Molecular view of adduct I at 290 K.	100
Figure 4.4B	Molecular view of adduct I at 195 K.	100
Figure 4.4C	Molecular view of adduct I at 100 K.	100
Figure 4.5A	Packing diagram of the adduct I at 290 K, viewed along the <i>a</i> -axis	101
Figure 4.5B	Packing diagram of the adduct I at 195 K, viewed along the <i>a</i> -axis	101
Figure 4.5C	Packing diagram of the adduct I at 100 K, viewed along the <i>a</i> -axis	102
Figure 4.5D	Packing diagram of the adduct I at 195 K, showing the extended-chains along [110]	102
Figure 4.5E	Packing diagram of the adduct I at 100 K, showing the 2-dimensional sheet	103
Figure 4.6	Graph of hydrogen bond density at temperatures 290, 195 and 100 K.	103
Figure 4.7	Plot of the scalar spontaneous strain, based on linear strains along the <i>a</i> -axis (e_1), <i>b</i> -axis (e_2), <i>c</i> -axis (e_3) and shear strain e_5 against temperature.	104
Figure 4.8	Plot of order parameter Q against temperature.	104
Figure 4.9	Schematic diagram of 2,4,4'-trimethoxybenzophenone	112
Figure 4.10	Graph of hydrogen bond density of 2,4,4'-trimethoxy benzophenone) at temperatures 297 and 100 K	119
Figure 4.11A	The molecular structure of 2,4,4'-trimethoxybenzophenone, at 297 K.	119
Figure 4.11B	The molecular structure of 2,4,4'-trimethoxybenzophenone, at 100 K.	120

Figure 4.12A	Packing diagram of the compound (II) at 297 K , viewed along the b-axis	120
Figure 4.12B	Packing diagram of the compound (II) at 100 K , viewed along the b-axis	121
Figure 4.12C	Packing diagram of the compound (II) at 297 K , viewed along the a-axis	122
Figure 4.12D	Packing diagram of the compound (II) at 100 K , viewed along the a-axis	123
Figure 4.13A	Temperature dependence of <i>c</i> -axis of compound (II).	129
Figure 4.13B	Temperature dependence of <i>a</i> - and <i>b</i> - axes of compound (II).	129
Figure 4.13C	Temperature dependence of angle β of the compound (II).	130
Figure 4.14	Temperature dependence of strain e_3 of 2,4,4'-trimethoxy benzophenone for $T \leq T_C$	130
Figure 4.15	Schematic diagram of 4-aminopyridinium 4-nitrobenzoic acid 4-nitrobenzoate	131
Figure 4.16	The molecular structure of 4-aminopyridinium, 4-nitro benzoic acid, 4-nitrobenzoate	135
Figure 4.17	The crystal packing of 4-aminopyridinium, 4-nitrobenzoic acid, 4-nitrobenzoate	136
Figure 4.18	Schematic diagram of 2-aminopyridinium 4-hydroxy benzoate	137
Figure 4.19	The molecular structure of 2-aminopyridinium 4-hydroxy benzoate	140
Figure 4.20	The crystal packing of 2-aminopyridinium 4-hydroxy benzoate	141
Figure 4.21	Schematic diagram of 3-aminobenzoic acid 4-nitrobenzoic acid (1/1)	142
Figure 4.22	The molecular structure of 3-aminobenzoic acid 4-nitro benzoic acid (1/1)	145
Figure 4.23	The crystal packing of 3-aminobenzoic acid 4-nitrobenzoic acid (1/1)	146

Figure 4.24	Schematic diagram of 2-amino-5-bromopyridine 4-hydroxy benzoic acid	147
Figure 4.25	The molecular structure of 2-amino-5-bromopyridine 4-hydroxybenzoic acid	151
Figure 4.26	The crystal structure of 2-amino-5-bromopyridine 4-hydroxybenzoic acid	152
Figure 4.27	Schematic diagram of 2-amino-4-methyl-pyridinium 3, 5-dinitrosalicylate	153
Figure 4.28	The molecular structure of 2-amino-4-methyl-pyridinium 3, 5-dinitrosalicylate	157
Figure 4.29	The crystal structure of 2-amino-4-methyl-pyridinium 3, 5-dinitrosalicylate	158
Figure 4.30	Schematic diagram of 2-amino-4-methylpyridinium 2-carboxybenzoate	159
Figure 4.31	The molecular structure of 2-amino-4-methylpyridinium 2-carboxybenzoate	162
Figure 4.32	The crystal structure of 2-amino-4-methylpyridinium 2-carboxybenzoate	163
Figure 4.33	Schematic diagram of bis(4-aminopyridinium) sulfate monohydrate	164
Figure 4.34	The molecular structure of bis(4-aminopyridinium) sulfate monohydrate	168
Figure 4.35	The crystal structure of bis(4-aminopyridinium) sulfate monohydrate	169
Figure 4.36	Schematic diagram of 2-amino-5-bromopyridinium 2-hydroxybenzoate	170
Figure 4.37	The molecular structure of the 2-amino-5-bromopyridinium 2-hydroxybenzoate	173
Figure 4.38	The crystal structure of 2-amino-5-bromopyridinium 2-hydroxybenzoate	174
Figure 4.39	Schematic diagram of 2-amino-5-methylpyridinium 2-hydroxybenzoate	175
Figure 4.40	The molecular structure of the 2-amino-5-methylpyridinium 2-hydroxybenzoate	178

Figure 4.41	The crystal structure of 2-amino-5-methylpyridinium 2-hydroxybenzoate	179
Figure 4.42	Schematic diagram of bis(2-amino-5-bromopyridinium) fumarate dihydrate.	180
Figure 4.43	The molecular structure of the bis(2-amino-5-bromopyridinium) fumarate dihydrate.	183
Figure 4.44	The crystal structure of bis(2-amino-5-bromopyridinium) fumarate dihydrate.	184
Figure 4.45	Schematic diagram of 2-amino-5-bromopyridinium 2-carboxybenzoate	185
Figure 4.46	The molecular structure of 2-amino-5-bromopyridinium 2-carboxybenzoate	189
Figure 4.47	The crystal structure of 2-amino-5-bromopyridinium 2-carboxybenzoate	189
Figure 4.48	Schematic diagram of 8-hydroxyquinolinium 2-carboxyacetate	190
Figure 4.49	The molecular structure of 8-hydroxyquinolinium 2-carboxyacetate	193
Figure 4.50	The crystal structure of 8-hydroxyquinolinium 2-carboxyacetate	194
Figure 4.51	Schematic diagram of quinoline-2-carbonitrile–fumaric acid (1/0.5)	195
Figure 4.52	The molecular structure of quinoline-2-carbonitrile–fumaric acid (1/0.5)	198
Figure 4.53	The crystal structure of quinoline-2-carbonitrile–fumaric acid (1/0.5)	199

LIST OF PHOTOGRAPHIC PLATES

	Page
Plate 1.1 Rotation photo for a good single crystal	8
Plate 3.1 SMART APEX II goniometer components (X-ray Crystallography Laboratory, School of Physics, USM)	60
Plate 3.2 SMART APEX II system (X-ray Crystallography Laboratory, School of Physics, USM)	60
Plate 3.3 SMART APEX II DUO system (X-ray Crystallography Laboratory, School of Physics, USM)	61
Plate 3.4 A sample prepared for X-ray crystallography	71

LIST OF ABBREVIATIONS

CCD	Charge-Coupled Device
R	Reliability Index
SADABS	Siemens Area Detector Absorption Correction
SAINT	SAX Area-detector Integration (SAX-Siemens Analytical X-ray)
SCI	Science Citation Index
SMART	Siemens Molecular Analysis Research Tools
wR	Weighted Reliability Index

**KAJIAN PERUBAHAN FASA BERSANDAR SUHU DAN PENGARUH
INTERAKSI IKATAN HIDROGEN KE ATAS MOD STRUKTUR DAN
PADATAN MOLEKUL ORGANIK DALAM KEADAAN HABLUR
TUNGGAL**

ABSTRAK

Dalam kajian ini, sebanyak lima belas sampel dalam keadaan hablur tunggal telah disediakan untuk penentuan struktur melalui kaedah kristalografi sinar-X hablur tunggal bagi tujuan mengkaji perubahan fasa yang disebabkan oleh ikatan hidrogen. Kajian perubahan fasa bersandar suhu melalui pembelauan sinar-X merupakan kaedah utama yang digunakan untuk mengkaji interaksi ikatan hidrogen dalam penyelidikan ini. Lima belas struktur hablur telah ditentukan dan mod susunan hablur tersebut juga telah dikaji. Cuma dua daripada lima belas sampel menunjukkan perubahan fasa yang telah diterangkan secara makroskopik dengan menggunakan teori Landau.

Ciri-ciri perubahan fasa daripada tiga polimorf suhu bagi ko-hablur hexamethylenetetraminium p-nitrobenzoate telah dikaji dengan eksperimen kristalografi sinar-X hablur tunggal pada tiga suhu yang berlainan dengan hablur yang sama. Ko-hablur mengalami pelbagai perubahan fasa daripada monoklinik Cm ke Cc (perubahan pertama) dan Cc ke Cc (perubahan kedua). Perubahan fasa ini adalah boleh-balik. Kedua-dua perubahan fasa digolongkan dalam darjah pertama, melibatkan pemutusan dan gandaan panjang paksi bagi paksi- c (suhu kritikal, T_c 259.5 K), paksi- a and paksi- b (suhu kritikal, T_c 182.5 K). Anion-anion p-nitrobenzoate adalah tidak tertib kecuali untuk fasa suhu rendah (100 K), menunjukkan perubahan fasa tertib-tidak tertib pada suhu perubahan 182.5 K.

Analisis struktur hablur untuk data yang dikumpul pada suhu 290 K menunjukkan bahawa hanya ada satu ikatan hidrogen intermolekul N—H...O manakala ia menunjukkan tiga dan empat belas ikatan hidrogen intermolekul N—H...O dan C—H...O pada masing-masing suhu 195 dan 100 K.

Hablur 2,4,4'-trimethoxybenzophenone mengalami perubahan fasa isomorf bersandar suhu boleh balik daripada monoklinik $P2_1$ pada suhu yang lebih tinggi daripada suhu kritikal (T_C) 154.5 K ke monoklinik $P2_1$ pada suhu lebih rendah dari T_C . Perubahan fasa ini digolongkan dalam darjah pertama dan melibatkan pemutusan dan hampir menggandakan panjang paksi- c pada suhu kritikal. Analisis struktur hablur untuk data yang dikumpul pada 297 K menunjukkan bahawa ada satu ikatan hidrogen intermolekul C—H...O manakala empat ikatan hidrogen intermolekul C—H...O ditemui pada suhu 100 K.

Ikatan hidrogen memainkan peranan penting dalam perubahan fasa ini sebagaimana ditunjukkan dengan pengurangan bilangan ikatan hidrogen apabila suhu dinaikkan.

**TEMPERATURE-DEPENDENT PHASE TRANSITION STUDIES AND
INFLUENCE OF HYDROGEN BONDING INTERACTIONS ON THE
STRUCTURAL AND PACKING MODES OF ORGANIC MOLECULES IN
SINGLE CRYSTALLINE STATE**

ABSTRACT

In this research, owing to the interests in phase transitions due to hydrogen bonds, fifteen samples with crystal structures and crystal networks that are utilizing the hydrogen bonding were prepared in single crystal form for X-ray structure determination. Temperature-dependent phase transitions studies by single crystal X-ray diffraction is the main experimental method used to study the hydrogen bonding interactions in this research. Fifteen crystal structures were determined and their crystal packing modes were also studied. Only two out of fifteen samples showed phase-transition which were explained macroscopically by Landau theory.

The phase transition behaviour of three temperature polymorphs of hexamethylenetetraminium p-nitrobenzoate co-crystal has been investigated by single crystal X-ray diffraction experiment at three different temperatures using the same crystal. The co-crystal undergoes multiple phase transitions from monoclinic *Cm* to *Cc* (first transition) and *Cc* to *Cc* (second transition). These transitions are reversible. Both of the phase transitions are of first order, involving the discontinuity and doubling of the *c*- and *a*-, *b*- axes at critical temperatures (T_C) 259.5 and 182.5 K, respectively. The p-nitrobenzoate anions are disordered except for the low temperature phase (100 K), displaying order-disorder phase transformation at transition temperature 182.5 K. The crystal structure analyses for data collected at 290 K show that there is only one intermolecular N—H...O hydrogen bond whereas

there are three and fourteen unique intermolecular N—H...O and C—H...O hydrogen bonds at temperatures 195 and 100 K, respectively.

The crystal of 2,4,4'-trimethoxybenzophenone undergoes a reversible temperature-dependent isomorphous phase transition from monoclinic $P2_1$ at temperature higher than the critical temperature (T_C) 154.5 K to another monoclinic $P2_1$ at temperature lower than T_C . The phase transition is of first order, involving the discontinuity and almost doubling of the c -axis at T_C . The crystal structure analyses for data collected at 297 K show that there is one intermolecular C—H...O hydrogen bond whereas there are four intermolecular C—H...O hydrogen bonds at the temperature 100 K.

The hydrogen bonding plays the pivotal role in these phase transitions as shown by the decrease of hydrogen bonding as the temperature is raised.

CHAPTER 1

INTRODUCTION

Owing to the interests in phase transitions due to hydrogen bonds, numerous crystalline forms of hydrogen bonded compounds were prepared for this study. With the change in temperature, some molecules with rich hydrogen bonding interactions undergo a reversible phase transition. The studies of first order phase transitions are ferroelastic in nature and have theoretically been described by Landau phenomenological ferroelastic theory approach. The core of this study is to investigate the influences of hydrogen bonding interactions on the structural and packing modes. Compounds with crystal structures and crystal networks which are utilizing the hydrogen bonding have been prepared in single crystal forms for X-ray structure determination. Structure determination by single crystal X-ray diffraction is the main experimental method used to study the hydrogen bonding interactions in this research. Single crystals are grown using slow evaporation technique for crystallization. Single crystal X-ray diffraction data are collected using SMART APEX II and APEX II DUO CCD diffractometers. The crystal structure is determined using direct methods. Various parameters describing the three-dimensional structures of these molecules (bond distances, bond angles, torsion angles, dihedral angles and *etc*) are calculated. Hydrogen bonding interactions between the molecules and its crystal packing mode are studied. Temperature-dependent phase transitions studies are conducted using the Oxford Cryosystem Cobra low-temperature attachment. The structural features of these compounds are compared with the related compounds from the Cambridge Crystallography Database Center.

1.1 General Introduction to Hydrogen Bonding and Other Interactions in the Crystalline State.

X-ray crystallography study is focused on the identification of molecular contents within the crystal solid state. Besides knowing the bonds angles and bond lengths within the asymmetric unit, we also obtained a whole host of information regarding to intra- and intermolecular interactions, for example: hydrogen bonds, C—H... Π interactions, short contacts and Π ... Π stacking interactions.

Good quality crystals suitable for single crystal X-ray diffraction studies are grown to study the nature of hydrogen bonding and other characteristic of the organic compounds. Hydrogen bonds and weak interactions play an important role in crystal structure packing. Some molecules with rich hydrogen bonding interactions exhibit temperature-dependent phase transitions (Chantrapromma *et al.*, 2006; Fun *et al.* 2003, 2007, 2010; How *et al.*, 2005; Usman *et al.*, 2001). Hydrogen bonds play a major role as steering forces to align molecules in crystal structures (Etter, 1990). The hydrogen bonding and weak interactions shall be studied experimentally with varying temperatures to explore the temperature dependencies of the spontaneous strain in the unit cell and also the crystal packing pattern obtained by single-crystal X-ray structure determination. However, it should be noted that to-date no confirmative guidelines have been laid down for finding what type of organic crystal would exhibit such phase transition. Taking these facts into considerations, in this research, focus shall be on temperature-dependent phase transition study negotiated by hydrogen bonding interactions. Molecular structures and packing modes of the rich hydrogen-bonded compounds are being evaluated (Etter & Frankenbach, 1989) as potential candidates.

In supramolecular chemistry, hydrogen bonding interactions are used to design the structures of molecular assemblies due to its adequately strong and directional behavior (Desiraju, 1995). In mechanistic biology, hydrogen bonding interactions play a significant role and functioning as base-pairing in nucleic acids as well as for the secondary and tertiary structures of proteins. Hydrogen bonds play a very important role in the DNA-molecule. It helps to hold the two strands of DNA together, helps antibodies to bind to antigens and also helps to bind enzymes to their substrates. Overall, it plays the role to assist the DNA-molecule to retain its shape and therefore maintain its life processes. Knowledge of hydrogen bond geometries, directionalities and motif formations is vital in the modeling of protein-ligand interactions in crystal engineering and supramolecular design.

Hydrogen bonding is a non-covalent interaction that involves donor and acceptor and can either be an intermolecular (between molecules) or intramolecular (between different parts of a molecule) bond. This kind of bonding can arise in both inorganic molecules, such as water, and organic molecules, such as DNA. Hydrogen bonding differs from other bonds because it is an extraordinary case of dipole forces. A hydrogen atom bonded to a relatively electronegative atom is a hydrogen-bond donor atom (Campbell *et al.*, 2006). Normally the electronegative atom is fluorine, nitrogen or oxygen, which has a partial negative charge. The hydrogen is bonded directly to the more electronegative element, causing the hydrogen atom to obtain a partial positive charge. Each of the atoms to which the hydrogen atom is bonded is not only significantly negative, but also has a minimum of one active lone pair to induce the dipole-dipole interactions. The hydrogen bond can be interpreted as a type of valence bond due to its partially covalent nature. It is directional, strong and interacts with a

limited number of electronegative partners (carbon, oxygen, nitrogen, sulfur, chloride and *etc* atoms).

An example of hydrogen bond table is presented in Table 1.1. $\sigma - H$ and $H \cdots \kappa$ are the covalent bond length and hydrogen bond length, respectively, where σ is hydrogen bond donor and κ represent hydrogen bond acceptor. These quantities characterize the hydrogen bond angle ($\sigma - H \cdots \kappa$). The ideal bond angle depends on the nature of the donor and acceptor atoms. The bond-lengths of hydrogen bond interactions vary according to the bond strength, temperature and pressure. Jeffrey (Jeffrey, 1997) categorizes hydrogen bonds into 3 groups (Table 1.2).

Table 1.1 Example of hydrogen bond table.

Hydrogen bond ($\sigma - H \cdots \kappa$)	Covalent bond length, Å ($\sigma - H$)	Hydrogen bond length, Å ($H \cdots \kappa$)	Hydrogen bond distance, Å ($\sigma \cdots \kappa$)	Hydrogen bond angle, ° ($\sigma - H \cdots \kappa$)
O1-H1O1...N1	0.81	1.94	2.752 (15)	148

Table 1.2 Properties of strong, moderate and weak hydrogen bonding interactions (Jeffrey, 1997).

	Strong interactions	Moderate interactions	Weak interactions
Hydrogen bond interactions	mostly covalent	partially of electrostatic and covalent	electrostatic
Bond lengths	$\sigma - H \approx H \cdots \kappa$	$\sigma - H < H \cdots \kappa$	$\sigma - H \ll H \cdots \kappa$
$H \cdots \kappa$ distances (Å)	1.2 – 1.5	1.5 – 2.2	2.2 – 3.2
$\sigma \cdots \kappa$ distances (Å)	2.2 – 2.5	2.5 – 3.2	3.2 – 4.0
Bond angles (°)	175 – 180	130 – 180	90 – 150
Bond energy (kcal mol ⁻¹)	14 – 40	4 – 15	< 4

Hydrogen bonds energies range from $< 4 \text{ kcal mol}^{-1}$ (for weak bond) to 40 kcal mol^{-1} (for extremely strong bond) and are dependent on the electronegativities of the donor and acceptor groups. Strong hydrogen bonding is known as “ionic hydrogen bonding” and always formed where there is shortage of donor group’s electron density or an excess acceptor group’s electron density, whereas moderate hydrogen bonding was formed by neutral donor and acceptor atoms. Typical enthalpies in vapor are presented in Table 1.3.

Table 1.3 Typical enthalpies of hydrogen bond (Jeffry, 1997).

F—H \cdots :F	40 kcal mol $^{-1}$
O—H \cdots :N	6.9 kcal mol $^{-1}$
O—H \cdots :O	5.0 kcal mol $^{-1}$
N—H \cdots :N	3.1 kcal mol $^{-1}$
N—H \cdots :O	1.9 kcal mol $^{-1}$

The hydrogen bond is very weak when compared to the covalent bond. However, the hydrogen bonded compound can still be stable and sufficiently strong when two or more hydrogen bonding interactions are formed between two molecules. It can be that a single hydrogen atom are involved in two or three hydrogen bonds (or even more) and are called as bifurcated or trifurcated hydrogen bonds, respectively. Such hydrogen bonds are formed in synthetic organic molecules. Etter, Bernstein and coworkers have introduced a language based upon graph-theory for describing and analyzing hydrogen bond networks in three-dimensional solids (Etter, 1990; Bernstein *et al.*, 1995). A generic graph-set descriptor is

$$G_d^a(n)$$

where G is the graph-set designator ($C/R/D/S$), d and a indicates number of donor and acceptor atoms, respectively. Total number of atoms present in the hydrogen bonded motif is presented by “ (n) ”. All hydrogen bonding patterns can be described in terms of chains (C), rings (R), dimer (D) and intramolecular hydrogen bonds (S). One of the benefits of using graph sets is that it brings into focus the hydrogen-bonded pattern and not simply on the geometrical constraints of these non-covalent interactions.

1.2 X-ray Crystallography Technique

X-ray crystallographic analysis is a powerful method for obtaining the atomic arrangements in the solid state and is a branch of science that deals with the three-dimensional structure of crystalline materials. The improvement in diffractometers and advancement in computers have greatly eased the data collection and structure determination.

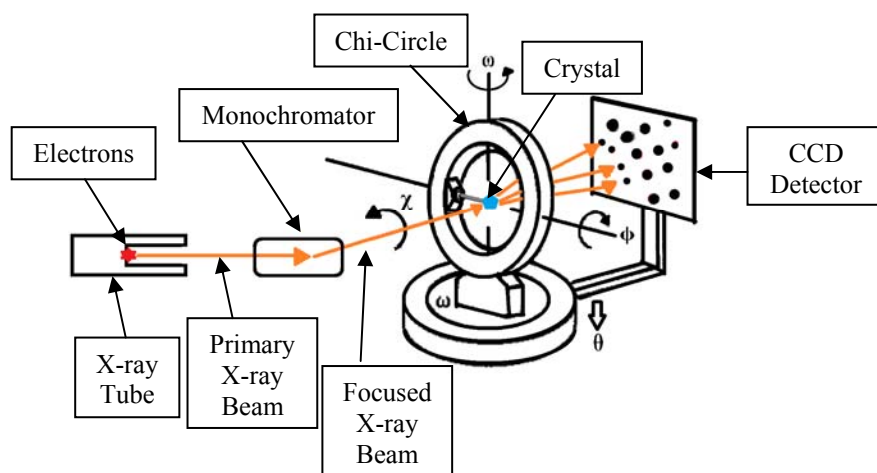


Figure 1.1 Diagram illustrating X-ray diffraction techniques.

To-date, X-ray crystallography technique is widely employed in the identification and structural confirmation of natural products and newly synthesized molecules in many fields such as physics, biology, chemistry, geology, mineralogy,

pharmacy and materials science. A diagram illustrating X-ray diffraction techniques is presented in Fig. 1.1.

Generally, the X-ray crystallographic structural determination in this study can be divided into four steps:-

(A) Crystal preparation.

Various techniques (slow evaporation, layering of miscible solvents) have been applied to grow good quality crystals suitable for data collection. Good crystals are selected under a microscope, and are mounted onto the goniometer head attached on the APEX II or APEX II DUO diffractometer. The mounted crystal must be optically aligned before data collection.

(B) Diffraction data collection.

A rotation photo (Plate 1.1) is taken to ensure good single crystal quality. 36 frames of data are then collected to obtain the unit cell. APEX II software is used to determine data collection strategy based on the unit cell. Diffraction data are collected from the mounted crystal during the data collection process.

(C) Data processing.

Integration and scaling are made after the data collection is over. *HKL* file consisting of reflection data was generated.

(D) Structures solving and three-dimensional molecular model construction.

Several attempts were done to obtain the final solution through *SHELXL* program. With the convergence of the refinement process, the crystal structure is considered to be solved and can be viewed in three-dimensional picture.

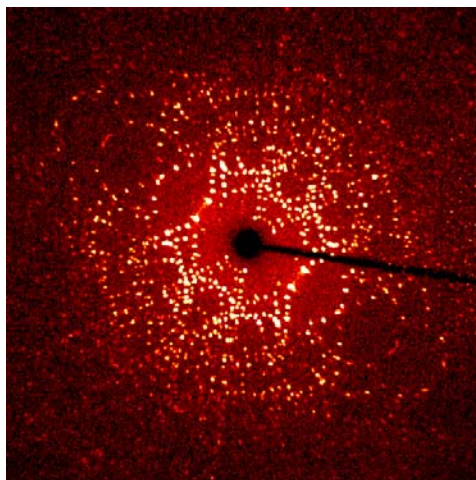


Plate 1.1 Rotation photo for a good single crystal.

X-ray single crystal structure determination is a solid state technique, the science of X-ray crystallography is based on the diffraction of X-rays by a crystalline material. X-ray can be diffracted from a single crystal due to its atoms being arranged in a periodic array over large atomic distances. Repetitive lattice containing the basis leads to a symmetric arrangement, with all information contained in the unit cell. Thus, the array can be extended by specifying the distance and angle to move from point to point by three primitive translational vectors \vec{a} , \vec{b} and \vec{c} . Once a unit cell has been chosen, parameters are used to identify the unit cell length (a, b, c) and angles (α, β, γ). The unit cell of an ideal single crystal will repeat in three-dimension with each basis fixed on each lattice point. Materials absent of systematic and long-atomic order arrangement are in non-crystalline (amorphous) forms and are not suitable for X-ray crystallography technique. Therefore, only single crystals are suitable to be used for this technique.

A single crystal exhibits symmetry operations as the result of the ordered internal arrangement of atoms and can be categorized into 7 crystal systems, 14 bravais lattices, 32 point groups and 230 space groups. The 7 lattice systems are triclinic, monoclinic,

orthorhombic, tetragonal, rhombohedral, hexagonal and cubic. Space group determination of the crystal is performed by narrowing down the choice of possible space group as much as possible. Systematic absences in the diffraction data and symmetry within the diffraction pattern are investigated to determine the space group.

In small molecular X-ray diffraction experiments, an intense beam of X-ray strikes the crystal under study. X-ray scattering is elastic; the outgoing X-rays have the same wavelength, and thus same energy, as the incident X-rays, only the direction is altered. Condition for constructive interference of scattered X-rays is given as

$$\Delta\vec{K} = \vec{G} \quad (1.1)$$

During X-ray diffraction, the electronic cloud causes the incoming X-ray to diffract in specific directions. The intensity of each reflection spot is measured. Each reflection spot is assigned to a set of Miller indices that identify the crystal planes that give rise to the reflection. Diagram illustrating Miller indices is presented in Fig. 1.2.

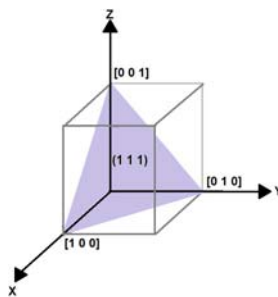


Figure 1.2 Diagram illustrating Miller indices.

The intensities of the reflections depend on the type of atoms within the unit cell whereas the positions of the reflections rely on the positions of the atoms in the crystal. A data set for a single crystal typically contains measurement of several hundreds of frames of data using the CCD diffractometers. These frames of data were integrated to generate the HKL intensity file. Another file generated during data collection contains information of the unit cell parameters and conditions during data collection. These two

files are to be used to solve the crystal structure using the SHELTXL software (Sheldrick, 2008).

An X-ray tube (Fig. 1.3) is used to emit the X-ray beam (electromagnetic radiation with the wavelength (λ) typically in the range of 0.1 to 100 Ångstroms) and consists of a metal target (anode) and a source of electrons (cathode). Characteristic X-ray is produced when an electron in an excited state jumps back to its ground state. Electrons are accelerated by high voltages after being discharged from the red-hot filament of the cathode and are allowed to collide with a metal target (anode). Most of the kinetic energy of the electrons is converted into heat after hitting the metal target. Water-cooling is necessary to dissipate the heat energy and prevent the metal target from melting. The bombarding electrons would knock electrons out of the inner shells of the target metal atom if these electrons have sufficient energy. X-ray photons with precise energies given by the difference between the electron energy levels are emitted after electrons from higher energy state fill these vacancies.

Continuous X-ray background are produced by bremsstrahlung.

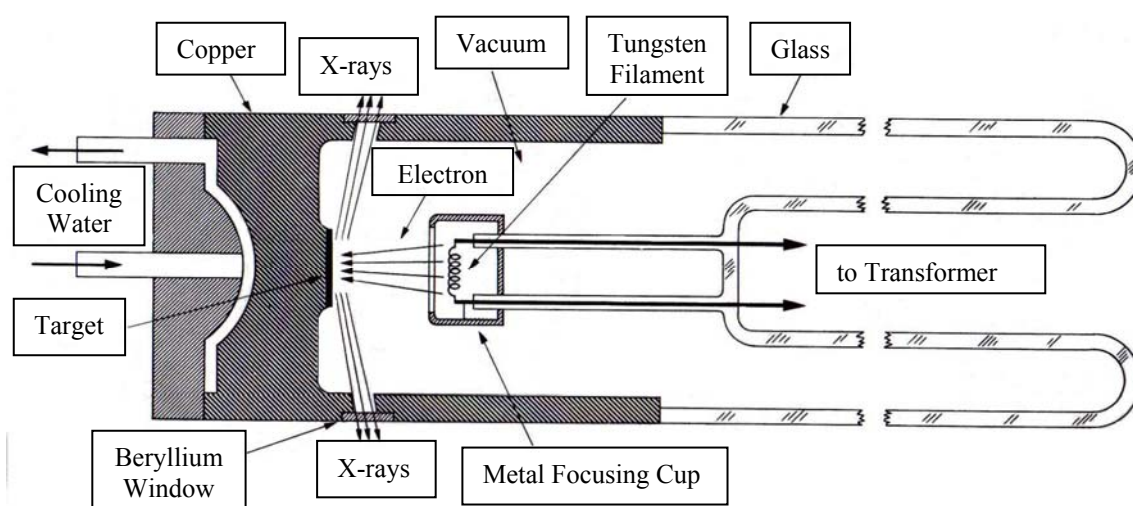


Figure 1.3 Cross section of filament X-ray tube (Cullity, 1967).

1.3 Brief Description on Phase Transition

The development of new materials with photoluminescent, ferroelectric, optoelectronic and other useful properties are important for science and modern technology (Bolstad & Diaz, 2002; Chandler *et al.*, 1993). These properties are related to the structural “order-disorder” phase transition of materials, and this area is generating much interest owing to the growing demand for new materials for specific technology applications (Longo *et al.*, 2007). Phase transition is the phenomenon where the single crystalline solid exhibits different molecular symmetries, for example, at different temperatures, pressure or under the applications of electric or magnetic fields. The principle of phase transition is investigated by kinetics, thermodynamics and magnetism; however our discussion here is based on structural order-disorder and isomorphous nature in solid state with varying temperatures (Longo *et al.*, 2007).

Phase transition is ubiquitous in nature, for example, occurring in crystals, magnets, liquid crystals and superconductor. A transition occurs when the equilibrium states of a system change qualitatively as a function of external imposed constraints. These constraints could be temperature, pressure, concentration, magnetic field or any number of other physical quantities. Understanding how to predict and describe both the existence of these transitions, as well as understanding their characteristics are important roles of condensed matter physics.

In this study, I proposed to outline one of the theoretical tools for describing phase transition, Landau phenomenological theory. Only transitions as a function of temperature will be considered in this study. In our cases, changes of unit cell parameters of single crystal as the function of temperature were observed, indicating that phase transitions are taking place in the crystals. These quantities are taken to be the

order parameters of the phase transitions. In the previous research project, a number of these phase transition samples have been found and have been published (How *et al.*, 2005; Chantrapromma *et al.*, 2006; Fun *et al.*, 2003, 2007, 2010)

Experimental findings of phase transition compounds are explained macroscopically by the Landau theory approach. Some of the phase transitions take place without any significant structural change. This kind of phase transition is known as isomorphous phase transition where the phase transition is not brought about by qualitative change such as crystal symmetry, but by quantitative change such as atomic size, amount of displacement or weight of atomic distribution (Gesi, 1976).

The abrupt jump in the unit cell lengths at the transition temperature is obviously a linear strain along the adjacent axis. Hence we assumed the dimensionless strain component along the adjacent axis, as the primary order parameter in the compound. The strain can be expressed as a power series expansion of the free energy of the crystal with respect to an order parameter of the crystal. Free energy and heat capacity are introduced to the crystal lattice changes through the Landau phenomenological Theory. The relationship between crystal thermodynamics and crystal lattice can show how the unit cell parameters changed under the influence of temperature and pressure (Stanley, 1971)

1.4 Samples Prepared for Phase Transition Studies

Owing to the interest in phase transitions due to hydrogen bonds, fifteen new compounds rich in hydrogen-bond interactions were synthesized and crystallized in X-ray laboratory, School of Physics, Universiti Sains Malaysia for this study. Two out of fifteen compounds have shown phase transitions in the temperature range of 90–290 K.

The previous studies of second order phase transitions (How *et al.*, 2005; Chantrapromma *et al.*, 2006; Fun *et al.*, 2003) are ferroelastic in nature and have theoretically been described macroscopically by Landau ferroelastic theory (Chantrapromma *et al.*, 2006; Fun *et al.*, 2003) and microscopically using the pseudo-spin approach (How *et al.*, 2005). First order reversible isomorphous phase transitions (Fun *et al.*, 2007, 2010) which are demonstrated macroscopically by Landau theory were also reported. All fourteen results have been published in SCI (Science citation indexed) publications.

1.4.1 Hexamethylenetetraminium P-nitrobenzoate (I)

Hexamethylenetetraminium (HMTA) compounds display excellent thermotropic structural phase transitions, depending on the chain length, disorder, twinning, modulated phases and hydrogen bonding (Pinheiro *et al.*, 2003). The sample structural phase transition report of HMTA has prompted us to synthesize and investigate the phase transition behaviour of the compound (I).

1.4.2 2,4,4'-Trimethoxybenzophenone (II)

Benzophenone crystals possess very good NLO (non-linear optics) and SHG (second harmonic generation) properties (Lammers *et al.*, 2000). Owing to our interest in phase transitions due to hydrogen bonds, we have prepared the crystalline forms of 2,4,4'-trimethoxybenzophenone. With the changing of the temperature, the compound (II) undergoes a first-order displacive reversible isomorphous phase transitions.

1.4.3 4-Aminopyridinium 4-Nitrobenzoic Acid 4-Nitrobenzoate (III)

4-Aminopyridine (Fampridine) is used clinically in Lambert-Eaton myasthenic syndrome and multiple sclerosis because by blocking potassium channels, it prolongs the action potentials thereby increasing transmitter release at the neuromuscular junction (Judge *et al.*, 2006; Schwid *et al.*, 1997; Strupp *et al.*, 2004). The crystal structure of 4-aminopyridine has been reported (Chao & Schempp, 1977; Anderson *et al.*, 2005). As an extension of our systematic study of hydrogen bonding patterns of 4-aminopyridine with aromatic carboxylic acids, we report here the crystal structure of the title compound.

1.4.4 2-Aminopyridinium 4-Hydroxybenzoate (IV)

2-Aminopyridine is used in the manufacture of pharmaceuticals, especially antihistaminic drugs (Windholz, 1976). As an extension of our systematic study of hydrogen bonding patterns of 2-aminopyridine with aromatic carboxylic acids, the title compound was synthesized and its crystal structure determined.

1.4.5 3-Aminobenzoic Acid 4-Nitrobenzoic Acid (1/1) (V)

3-Aminobenzoic acid is used as an intermediate for dyes, pesticides and in other organic synthesis (Windholz, 1976). The crystal structures of 3-aminobenzoic acid (Voogd *et al.*, 1980) and 4-aminobenzoic acid-4-nitrobenzoic acid have been reported (Bowers *et al.*, 2005). As a part of our investigation of the hydrogen bonding interaction between acids, we report herein the crystal structure of the title compound.

1.4.6 2-Amino-5-bromopyridine 4-Hydroxybenzoic Acid (VI)

Pyridine and its derivatives play an important role in heterocyclic chemistry (Pozharski *et al.*, 1997; Katritzky *et al.*, 1996). They are often involved in hydrogen-bond interactions (Jeffrey & Saenger, 1991; Jeffrey, 1997; Scheiner, 1997). 4-Hydroxybenzoic acid is a good hydrogen-bond donor and can form co-crystals with other organic molecules (Vishweshwar *et al.*, 2003). We have recently reported the crystal structures of 2-amino-5-bromopyridine-benzoic acid (Hemamalini & Fun, 2010a), 2-amino-5-bromopyridinium 3-aminobenzoate (Hemamalini & Fun, 2010b) and 2-amino-5-bromopyridinium hydrogen succinate (Hemamalini & Fun, 2010c) from our laboratory. In continuation of our studies of hydrogen bonding patterns of pyridinium derivatives, the crystal structure determination of the title compound has been undertaken.

1.4.7 2-Amino-4-methyl-pyridinium 3, 5-Dinitrosalicylate (VII)

Pyridine and its derivatives play an important role in heterocyclic chemistry (Pozharski *et al.*, 1997; Katritzky *et al.*, 1996). They are often involved in hydrogen-bond interactions (Jeffrey & Saenger, 1991; Jeffrey, 1997; Scheiner, 1997). There are numerous examples of 2-amino-substituted pyridine compounds in which the 2-aminopyridines act as neutral ligands (Navarro Ranninger *et al.*, 1985; Qin *et al.*, 1999; Ren *et al.*, 2002; Rivas *et al.*, 2003) or as protonated cations (Luque *et al.*, 1997; Jin *et al.*, 2001; Albrecht *et al.*, 2003). The nitrosubstituted aromatic acid 3,5-dinitro salicylic acid (DNSA) has proven potential for formation of proton-transfer compounds, particularly because of its acid strength ($pK_a = 2.18$), its interactive *ortho*-related phenolic substituent group together with the nitro substituents which have potential for

both $\pi\cdots\pi$ interactions as well as hydrogen-bonding interactions. A large number of both neutral and proton-transfer compounds of Lewis bases with DNSA, together with their IR spectra have been reported (Hindawey *et al.*, 1980; Issa *et al.*, 1981) in the literature. Since our aim is to study some interesting hydrogen bonding interactions, the crystal structure of the title compound is presented here.

1.4.8 2-Amino-4-methylpyridinium 2-Carboxybenzoate (VIII)

Pyridine and its derivatives play an important role in heterocyclic chemistry (Pozharski *et al.*, 1997; Katritzky *et al.*, 1996). They are often involved in hydrogen-bond interactions (Jeffrey & Saenger, 1991; Jeffrey, 1997; Scheiner, 1997). Since our aim is to study some interesting hydrogen-bonding interactions, the crystal structure of the title compound, (VIII), is presented here.

1.4.9 Bis (4-aminopyridinium) Sulfate Monohydrate (IX)

4-Aminopyridine (fampridine) is clinically used in the treatment of Lambert-Eaton myasthenic syndrome and multiple sclerosis. It prolongs action potentials by blocking potassium channels, thereby increases transmitter release at the neuromuscular junction (Judge & Bever, 2006; Schwid *et al.*, 1997; Strupp *et al.*, 2004). Hydrogen bonding patterns involving sulfate and sulfonate groups in biological systems and metal complexes are also of current interest (Onoda *et al.*, 2001). Benzoic acid and sulfuric acid form a stable hydrogen-bonded complex that favors aerosol formation in the atmosphere (Zhang *et al.*, 2004). In a sulfate-binding protein, the sulfate anion is mainly bounded by seven hydrogen bonds, five of which are from the main chain peptide NH

groups (Pflugrath & Quioco, 1985; Jacobson & Quioco, 1988). The present study is aimed at understanding the hydrogen bonding networks in the title compound (IX).

1.4.10 2-Amino-5-bromopyridinium 2-Hydroxybenzoate (X)

Recently, much attention has been devoted to the design and synthesis of supramolecular architectures assembled via various weak noncovalent interactions, such as hydrogen bonds, $\pi\cdots\pi$ stacking and C—H $\cdots\pi$ interactions (Remenar *et al.*, 2003; Sokolov *et al.*, 2006). Salicylic acid (SA) plays a central role in resistance and defense induction in response to pathogen attack and its role in the activation of the hypersensitive response (HR), a form of programmed cell death associated with resistance of plants. Mutants or transgenic plants impaired with the accumulation of SA cannot mount efficient defense responses to pathogens after infection (Sticher *et al.*, 1997). SA depletion by transgenic expression of a bacterial SA hydroxylase encoded by NahG abolishes local and systemic resistance responses to various pathogens (Rairdan & Delaney, 2002). This has been confirmed by the use of Arabidopsis mutants impaired in SA accumulation after pathogen infection (*sid1/eds5*, *sid2*), showing higher susceptibility to fungal and bacterial pathogens (Nawrath & Métraux 1999; Wildermuth *et al.*, 2001). The present study is aimed at understanding the hydrogen-bonding networks in the title compound, (X).

1.4.11 2-Amino-5-methylpyridinium 2-Hydroxybenzoate (XI)

Hydrogen bonding has been established as the most effective tool for constructing sophisticated assemblies because of its strength and directionality. Carboxylic acids are believed to have existed in the prebiotic earth (Miller & Orgel,

1974; Kvenvolden *et al.*, 1971) and they exhibit characteristic intermolecular interactions and aggregation patterns. Carboxyl groups have been used as primary building blocks in the design of crystal structures (Desiraju, 1989; MacDonald & Whitesides, 1994). Salicylic acid, a well known analgesic, and its complexes with a few drug molecules such as antipyrine (Singh & Vijayan, 1974) and sulfadimidine (Patel *et al.*, 1988) were already reported in the literature. The present study is aimed at investigating the supramolecular interactions of the title compound, (XI).

1.4.12 Bis(2-amino-5-bromopyridinium) Fumarate Dihydrate (XII)

Hydrogen bonding plays a key role in molecular recognition (Goswami & Ghosh, 1997) and crystal engineering research (Goswami *et al.*, 1998). Fumaric acid, the *E* isomer of butenedioic acid, is of interest since it is known to form supramolecular assemblies with *N*-aromatic compounds (Batchelor *et al.*, 2000). It tends to form infinite chains arranged in a nearly coplanar manner via pairs of strong O—H \cdots O hydrogen bonds. The crystal structures of 2-aminopyridinium-fumarate-fumaric acid (2/1/1) (Büyükgüngör *et al.*, 2004) and 2,6-diamino pyridinium hydrogen fumarate (Büyükgüngör & Odabasoglu, 2006) have been reported in the literature. In order to study some interesting hydrogen bonding interactions, the synthesis and structure of the title compound, (XII), is presented here.

1.4.13 2-Amino-5-bromopyridinium 2-Carboxybenzoate (XIII)

Phthalic acid forms hydrogen phthalate salts with various organic and other compounds. The crystal structures of hydrogen phthalates including calcium phthalate monohydrate (Schuckmann *et al.*, 1978), lithium hydrogen phthalate monohydrate

(Kuppers *et al.*, 1985) and tetramethylammonium hydrogen phthalate (Jessen, 1990) have been reported in the literature. Hydrogen phthalates also form supramolecular assemblies, such as extended chains, ribbons and three-dimensional networks (Dale *et al.*, 2004; Ballabh *et al.*, 2005). The hydrogen-bonding patterns of 2-amino-5-bromopyridinium hydrogenphthalate, (XII), are discussed.

1.4.14 8-Hydroxyquinolinium 2-Carboxyacetate (XIV)

Recently, much attention has been devoted to the design and synthesis of supramolecular architectures assembled *via* various weak non-covalent interactions in the crystal structures of oxines (8-hydroxyquinoline), their derivatives and their complexes in a variety of crystalline environments (Balasubramanian & Thomas Muthiah, 1996*a, b*). Oxine is widely used as analytical reagent. The present study is aimed at understanding the hydrogen bonding networks in the title compound (XIV).

1.4.15 Quinoline-2-carbonitrile-fumaric Acid (1/0.5) (XV)

Heterocyclic molecules containing the cyano group are useful as drug intermediates. Syntheses of quinoline derivatives have been discussed earlier (Sasaki *et al.*, 1998; Reux *et al.*, 2009). In continuation of our previous work, we have synthesized a quinoline compound to investigate its hydrogen bonding patterns.

1.5 Research Objectives

The objective of this study is to improve the present understanding of the hydrogen- bonds-driven-phase transition by analyzing the crystal structure, crystal packing and hydrogen bonding patterns. Fifteen hydrogen-bonding rich compounds

were synthesized to fulfill this objective. Three-dimensional picture of the crystal structures are determined through X-ray crystallography technique. This technique provides detailed information of the molecular view, geometrical parameters, solid state packing and hydrogen bond patterns. Hydrogen bonding interactions between the molecules in the solid state were studied. The pivotal roles of hydrogen bonds in phase transition nature are also investigated in this study. The structural features of these compounds are compared with the related compounds from CCDC (Cambridge Crystallography Data Center). Phase transition test are performed in all the prepared samples by examining the crystal system and cell parameters in both low (100K) and room temperature (290K). All parameters, geometries and changes in symmetries of samples which exhibit the phase transition at different temperatures were further investigated. In addition, Landau phenomenological theory approach is used to explain these experimental findings.

CHAPTER 2

FUNDAMENTAL OF X-RAY STRUCTURE ANALYSIS

2.1 X-ray Diffraction

X-ray crystallography technique is based on the interaction between X-ray and crystal lattice and was explained by Bragg's Law. Crystal lattice diffracts the X-ray and the X-ray diffraction pattern is recorded by CCD. The intensities of points in reciprocal space are recorded during data collection process and used to generate an electron density map (real space). The theory and consequence of X-ray diffraction of crystals is discussed in this chapter. Diffraction occurs whenever Bragg's law is fulfilled and can be defined as a combination of interference and scattering phenomenon (Ladd & Palmer, 1993). From Fig 2.1, parallel incident rays, A and B , make an angle, θ , with planes P_1 and P_2 . The parallel reflections rays A' and B' are produced as a result of interference with the condition that both waves are in phase. Electrons at W and Y are triggered by the oscillating field of incident X-ray to vibrate and scatter in all directions.

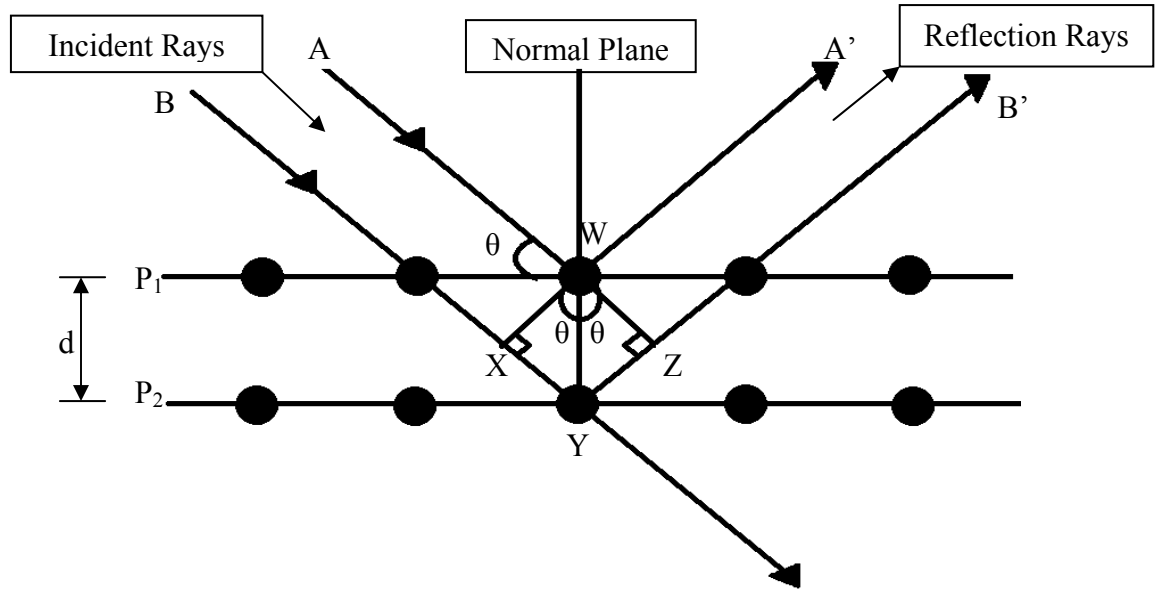


Figure 2.1 Diagram illustrating X-ray diffraction

Fig. 2.1 displays only two parallel lattice planes (P_1, P_2) and the path difference is labeled as d (d-spacing). The two parallel secondary rays (A', B') will reflect at angle θ . A diffracted beam of peak intensity is produced if the waves illustrated by these rays are in phase. It is clear that $\Delta XWY = \Delta ZWY = \theta$ and $XY = YZ$. The difference in path lengths,

$$XY + YZ = 2XY \quad (2.1)$$

is equivalent to an integral number (n) of wavelengths (λ) and is represented by

$$2XY = n\lambda \quad (2.2)$$

By substitution $\frac{XY}{d} = \sin \theta$ (Fig. 2.1) in equation (2.2), we get Bragg's law,

$$2d \sin \theta = n\lambda \quad (2.3)$$

2.2 Intensity of Reflections

The intensities and the coordinate of reflections are measured with a CCD diffractometer. Each measured diffraction spot is associated to the corresponding Miller indices (h,k,l) and has an value of intensity. The intensity of a diffraction spot is proportional to the square of the structure factor amplitude ($|F(hkl)|$). On a diffraction pattern, each diffraction spot has associated with the amplitude and direction of the diffracted beam.

2.3 Atomic Scattering Factors

The incident X-rays interacted with and subsequently are scattered by the electrons in the atom. Atomic scattering factors (atomic form factors) are the amplitudes of X-ray waves scattered from an atom. As the wavelength of the X-ray is of the order of the atom diameter, most of the scattering is in the forward direction. The atomic scattering factors are formulated as functions of $\frac{\sin \theta}{\lambda}$ and usually expressed as $f_{j, \theta}$. It is a function of the scattering direction, wavelength of X-rays used, nature and thermal vibrations of the atom. As the X-rays are scattered by the electrons in the atom, it is obvious that the X-ray scattering power is directly proportional to the atomic number in the particular atom. Atomic scattering factors are related to the Bragg angle (Fig. 2.2). The X-ray scattering power is a function of Bragg angle and decreases with wider Bragg angle and is greater for heavier atoms. The atomic scattering factors of carbon (five electrons) are significant different from lead (eighty two electrons). The reduction of the atomic scattering factors at high Bragg angles occurs more gradually. The value of f equals to the number of electrons for zero scattering angle [$\sin \theta (hkl) = 0$]

$$f_{j,\theta(\theta=0)} = Z_j \quad (2.4)$$

where f is measured in electrons.

Anomalous dispersion effects (characteristically resonance absorption) which become substantial in the vicinity of the X-ray absorption edge of the scattering atom also contribute to the scattering factor.

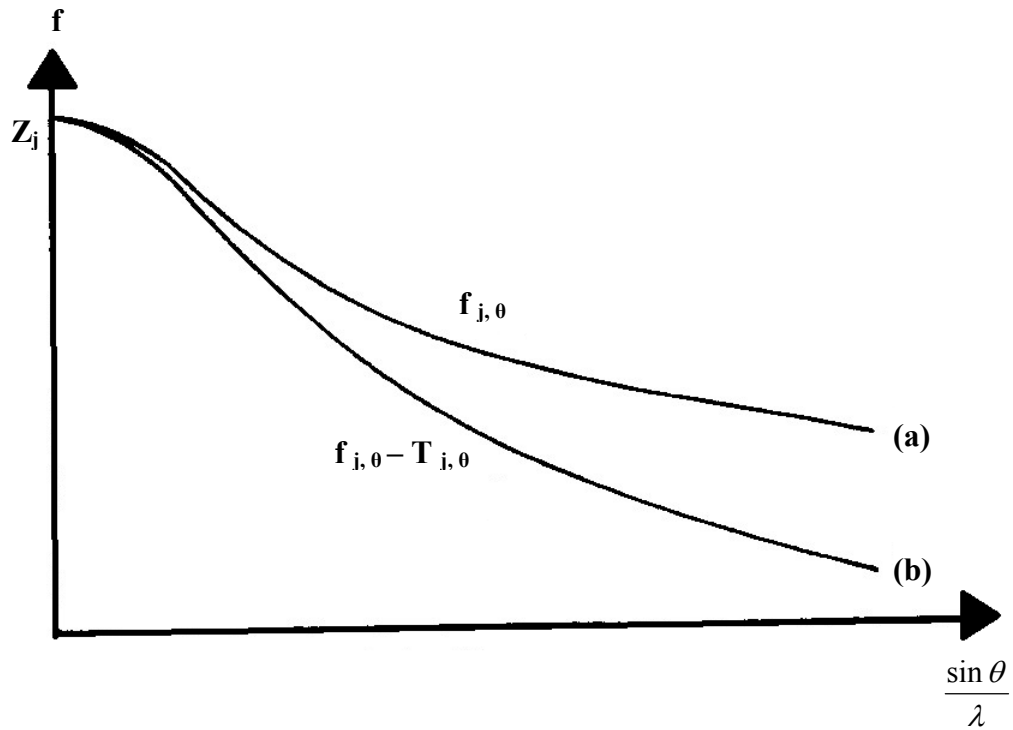


Figure 2.2 Atomic scattering factors (a) stationary atom, $f_{j,\theta}$ (b) atom corrected for thermal vibration, $f_{j,\theta} - T_{j,\theta}$. (Ladd & Palmer, 1993).

The fall-off in intensity with increasing scattering angle increases with the increase in the vibrations of atoms, and these vibrations increase with higher temperature. By considering isotropic vibration, a general expression for the temperature factor correction to the atomic scattering factor for the j th atom is

$$T_{j,\theta} = \exp\left[-B_j\left(\frac{\sin^2\theta}{\lambda^2}\right)\right] \quad (2.5)$$

where B_j is the temperature factor of the j th atom and can be associated to the mean displacement of a vibrating atom $\overline{U_j^2}$ by the Debye-Waller equation

$$B_j = 8\pi^2 \overline{U_j^2} \quad (2.6)$$

$\overline{U_j^2}$ is a function of temperature and represents the mean square amplitude of vibration of the j th atom from its equilibrium position in a direction normal to the reflecting plane.

The temperature-corrected atomic scattering factor is a function of $\frac{\sin\theta}{\lambda}$ and is given by

$$g_j = f_{j,\theta} T_{j,\theta} \quad (2.7)$$

2.4 Argand Diagram

The combined wave can be clearly and concisely expressed as vectors with imaginary and real components in an Argand diagram and is given as

$$\mathbf{F} = \mathbf{f}_1 + \mathbf{f}_2 \quad (2.8)$$

where

$$f_1 = f_1 \cos \phi_1 + i(f_1 \sin \phi_1) \quad (2.9)$$

$$f_2 = f_2 \cos \phi_2 + i(f_2 \sin \phi_2) \quad (2.10)$$

These equations are illustrated in Fig. 2.3.